Pergamon

Chemical Engineering Science, Vol. 53, No. 6, pp. 1131–1144, 1998

Printed in Great Britain

PII: S0009-2509(97)00410-7

0009-2509/98 $19.00 + 0.00

The rheology and processing of a concentrated cellulose acetate solution

W.-K. Wee and M. R. Mackley*

Department of Chemical Engineering, University of Cambridge, Cambridge CB2 3RA, U.K.

(Received 11 June 1997; in revised form 28 October 1997; accepted 13 November 1997)

Abstract—This paper develops an experimental protocol for the characterisation of a concentrated cellulose acetate solution using a viscoelastic integral constitutive equation. Rheological parameters are obtained from both a Rheometrics RDSII spectrometer and a newly developed Multipass Rheometer (MPR). Reasonable self-consistency is found between machines and model. A numerical simulation of the MPR processing flow is carried out using Polyflow and the integral constitutive equation and the results are compared with the experimental data. In general, the fit is found to be good and we conclude that the modelling approach adopted here is capable of predicting the viscoelastic processing flow of concentrated polymer solutions with reasonable accuracy. The MPR is also shown to be a useful machine for the study of systems containing volatile fluids. © 1998 Elsevier Science Ltd. All rights reserved.

Keywords: Concentrated cellulose acetate solution; multi-pass rheometer; rheological characterisation; processing behaviour; wagner integral equation; numerical simulation.

INTRODUCTION

Cellulose acetate is widely used in the manufacturing of textiles and other fibres. However, being an intractable polymer in its pure molten form, it is usually processed as a concentrated solution with a typical solid weight fraction of about 20–30%. Acetone is the most common solvent used for cellulose acetate in the dry fibre spinning process which converts the polymer solution into fibres, although methylene chloride is an alternative solvent. In the fibre-spinning operation, a solution of the polymer in the volatile solvent is forced through a spinneret into a cabinet of warm air and the fibres are formed by evaporation of the solvent. A number of process areas are important in the manufacturing of fibres and these include the formation of the spinning solution, the upstream rheological and flow behaviour of the solution and the solvent loss during fibre formation [see, for example, Griswold and Cuculo (1974)].

This paper concentrates on the upstream rheological and processing behaviour of the concentrated solution which presents a difficulty for this particular system because the cellulose acetate–acetone solution is volatile and makes rheological measurements using conventional equipment difficult. The rheology of cellulose acetate–acetone solution has been studied by a number of people and in these papers the material or its derivatives were either characterised as a power-law fluid or the non-linear response described by a multi-parameter apparent viscosity. Johnston and Sourirajan (1973) investigated the relationship between limiting viscosity number and average molecular mass of solutions of cellulose acetate in acetone by using Mark–Houwink equation over a range of temperatures. Moore and Brown (1959) studied the viscosity-temperature data for dilute solutions of cellulose derivatives in a similar manner. Griswold and Cuculo (1974) correlated the rheological data of concentrated cellulose acetate–acetone system obtained from an Instron capillary rheometer to the spinnability in the dry-spinning process and Wang and Fried (1992) published a paper concerned with the viscoelastic properties of concentrated cellulose acetate solutions in different solvents but not in acetone.

In this paper we describe a rheological protocol that enables the rheological and processing measurements of concentrated cellulose acetate–acetone solution to be made. Both the small strain linear viscoelasticity and large strain non-linear viscoelastic response has been measured quantitatively using a special protocol in a conventional Rheometrics Dynamics Spectrometer (RDSII). A K-BKZ constitutive equation with a strain-dependent damping function, which was originally developed for polyethylene melts [see, for example, Laun (1978), Wagner (1976) and Wagner (1979)] has been used to characterise the

*Corresponding author.

fluid. An important aspect in relation to this model is that the constitutive equation is separable in terms of time and strain dependence. This particular model has been applied and shown to give good agreement for a range of fluids [see e.g. Mackley *et al.* (1994)], but has yet to be used for concentrated polymer solutions. The present work establishes the validity of this equation in describing the rheological response of concentrated cellulose acetate–acetone solutions.

This paper also describes results on concentrated cellulose acetate solutions obtained using a newly developed Multi-Pass Rheometer (MPR) [Mackley *et al.* (1995)]. Rheological measurements have been carried out using this new apparatus and reasonable self-consistency with the RDSII data is obtained. The MPR study also includes processing experiments at typical engineering processing temperatures, shear rates and pressures. The fully enclosed system of the MPR presents an improved way of measuring the steady flow response for volatile and sensitive materials such as cellulose acetate solutions.

In addition to experimental rheological and processing measurements we have tested our characterisation by using a numerical software package Polyflow in order to predict the process behaviour of the concentrated polymer solution for MPR experiments. The simulation was accomplished by combining the Wagner constitutive equation, the experimental boundary conditions and the experimental viscoelastic parameters.

2. RHEOLOGICAL BACKGROUND AND SIMPLE SHEAR CHARACTERISATION

The constitutive equation chosen was a K-BKZ equation of the separable type with a single parameter exponential damping function as proposed by Wagner (1976). This particular damping function was chosen because of its effectiveness and simplicity although many other forms have been proposed [see, for example, Laun (1978), Papanastasiou *et al.* (1983), Soskey and Winter (1984) and Booij and Palmen (1982)]. The equation can be expressed for simple shear in the following form:

$$\tau(t) = -\int_{-\infty}^{t} \sum_i \frac{g_i}{\lambda_i} e^{-(t-t')/\lambda_i} e^{-k\gamma(t,t')} \gamma(t,t')\,dt' \quad (1)$$

where $\tau(t)$ is the stress at a current time t, g_i and λ_i are the relaxation strength and the relaxation time of the polymer respectively, and k the damping factor or coefficient which quantifies the level of non-linearity in the material empirically; $\gamma(t,t')$ is the past strain defined between t and t' as

$$\gamma(t,t') = \int_{t}^{t} \dot{\gamma}(t'')\,dt''. \quad (2)$$

The above constitutive equation is factorized in terms of the time and strain dependence of the polymer. The strain dependence of the fluid is contained within the damping function whereas the material's time dependence is contained within the relaxation modulus term with g_i and λ_i. In order to apply eq. (1), we determine the relaxation spectra (g_i, λ_i) from the linear oscillatory dynamic storage and loss moduli by means of Rheometrics software and the damping coefficient from linear and non-linear step-strain experimental results [see, for example, Mackley *et al.* (1994)].

In the linear or small strain region, Ferry (1980) amongst others showed that eq. (1) leads to the following expressions for the oscillatory storage and loss moduli G' and G'' as functions of angular frequency, relaxation time and relaxation strength:

$$G'(\omega_j) = \sum_i \frac{g_i \lambda_i^2 \omega_j^2}{(1 + \lambda_i^2 \omega_j^2)} \quad (3)$$

$$G''(\omega_j) = \sum_i \frac{g_i \lambda_i \omega_j}{(1 + \lambda_i^2 \omega_j^2)}. \quad (4)$$

The index j represents the experimental data points ($j = 1 \rightarrow N$) and i represents the data points of the spectrum ($i = 1 \rightarrow M$). G' and G'' represent the elastic and viscous contributions to the properties of the fluid and these two equations allow us to obtain the discrete relaxation spectrum from oscillatory shear measurements. From experience with other rheological characterisation we are confident that an adequate fit to the linear viscoelastic data can be achieved using 8–11 time constants logarithmically spaced from one another [see, for example, Aldhouse *et al.* (1986) and Baumgaertel and Winter (1989)]. A complex viscosity $\eta^*(\omega)$, defined by

$$\eta^*(\omega) = \frac{1}{\omega}\sqrt{G'^2 + G''^2} \quad (5)$$

is, therefore, given by

$$\eta^*(\omega) = \sum_i \frac{g_i \lambda_i}{\sqrt{(1 + \lambda_i^2 \omega^2)}}. \quad (6)$$

An analogy between the complex viscosity η^* and the steady-flow viscosity η can be made. On a purely empirical basis, Cox and Merz (1958) suggested that η^* and η are the same when compared at equal values of frequency and shear rate:

$$\eta^*(\omega) = \eta(\dot{\gamma}) \quad \text{at} \quad \omega = \dot{\gamma}. \quad (7)$$

While not exact, eq. (7), also known as the Cox–Merz rule, appears to be at least a reasonable approximation for many polymer systems.

Step strain is an important test used to generate the constitutive parameter in terms of the damping function. The extent of which time-strain separability holds can be estimated by examining the step shear strain relaxation modulus at both linear and non-linear strains. In a step strain and relaxation experiment a shear strain is induced by applying a constant shear rate for a short interval and the stress is measured as a function of time. More commonly, the material function that is measured is the relaxation

modulus $G(\gamma_1, t) = \tau(t)/\gamma_1$. In step-strain measurements, the strain history can be represented by

$$\text{for } t < 0, \quad \gamma = -\gamma_1$$

$$\text{for } t > 0, \quad \gamma = 0.$$

Substituting this into eq. (1) and evaluating the integral yields the following expression which illustrates the separability of time and strain dependence:

$$\begin{aligned} G(t, \gamma_1) &= \tau(t)/\gamma_1 \\ &= \sum_i g_i e^{-t/\lambda_i} \cdot e^{-k|\gamma_1|} \\ &= G(t, \gamma_0) e^{-k|\gamma_1|} \end{aligned} \tag{8}$$

where $G(t,\gamma_0)$ is the linear relaxation modulus measured at a small strain γ_0. The damping function for the polymer can be readily obtained from eq. (8) using experimental step-strain data. At a given time, using a log–log plot, we determine the ratio of the relaxation modulus at non-linear strain, $G(t, \gamma_1)$, to the modulus at linear strain, $G(t, \gamma_0)$. Substitution of the values of the moduli in eq. (8) provides the Wagner damping function from which an exponential fit to the data generates the damping coefficient, k.

In steady shear flow, Mackley *et al.* (1994) shows that an analytical expression of the shear stress τ as a function of the steady shear rate can be obtained from eq. (1) in the following form:

$$\tau(\dot{\gamma}) = \sum_i \frac{g_i \lambda_i \dot{\gamma}}{(1 + k\lambda_i \dot{\gamma})^2}. \tag{9}$$

By substituting the values of the relaxation spectrum and damping coefficient into eq. (9), a comparison between this prediction with actual experimental shear data can be achieved and the extent to which the model is successful is then tested.

EXPERIMENTAL PROTOCOL

Controlled strain measurements on the Rheometrics Dynamics Spectrometer were performed at 20°C in a cone and plate geometry with plate diameter of 25 mm and gap of 0.08 mm. A force rebalance transducer with full scale torque capacity of 100 g cm (0.01 Nm) was fitted to the rheometer. The polymer solution used contains 25.4 wt% cellulose acetate, 71.1 wt% acetone and 3.5 wt% water. The solution was prepared by Courtaulds and syringed into either the Rheometrics RDSII or the Multi-Pass Rheometer. The number and weight average molecular mass of the polymer was not known with precision. We chose to look at this concentration because it lies in the middle of the range of concentrations which are of practical interest to processors of cellulose acetate. The material parameters for eq. (1) are determined using a standard procedure as follows. A series of strain sweep measurements were carried out at a fixed frequency to establish the region for which the material behaves linearly. By use of on-line Rheometrics software, the discrete relaxation spectrum, (g_i, λ_i) was obtained from the linear oscillatory measurements, $G'(\omega)$ and $G''(\omega)$. Eight time constants were used for the present study. The damping coefficient k was determined from the step-strain relaxation moduli in both the linear and non-linear domains.

For this polymer system, a special protocol had to be developed to reduce the rate of evaporation of the acetone from the sample upon exposure to its environment. A layer of 'skin' will otherwise be formed on the sample's surface due to rapid acetone evaporation rendering the measurements unreliable. The protocol involves saturating the test area with acetone vapour before commencing the experiment. In addition, a thin layer of silicon was smeared on top of the exposed surface of the sample to cut off its contact with the surrounding air as shown in Fig. 1.

The effect of the 'skin' phenomenon is illustrated by performing a time sweep experiment, i.e., tracing the changes in the dynamic moduli G' and G'' with respect to time. A strain of 10% at a fixed frequency of 10 rad/s was chosen for the test. The time sweep was first performed under normal condition and then repeated with the attempt to reduce the acetone evaporation by the developed protocol. It can be seen in

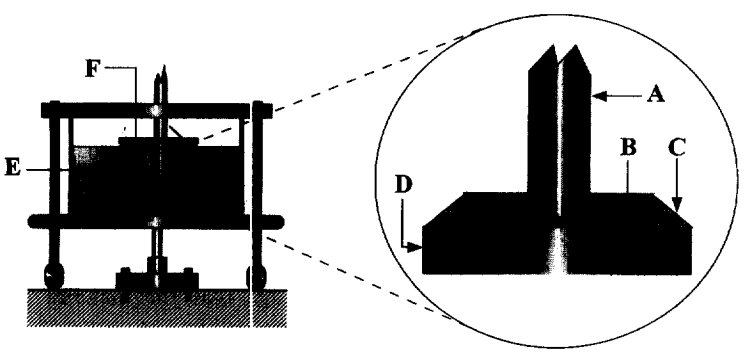

Fig. 1. Schematic diagram of the Rheometrics RDSII mechanical spectrometer operating with cone and plate at 0.08 mm gap. A. 25 mm cone, B. concentrated cellulose acetate solution, C. thin silicon oil coating, D. lower fitting that is driven by stepper motor, E. ethylene glycol bath set at 20°C, F. test environment saturated with acetone vapour.

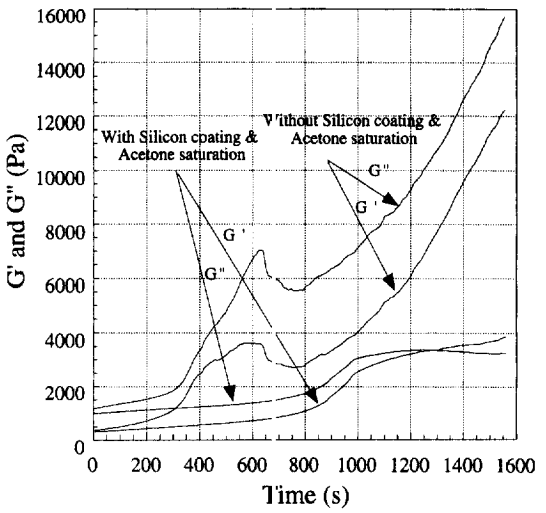

Fig. 2. RDSII oscillatory measurements on 25.5 wt% cellulose acetate-acetone solution at 20°C, G' and G'' as a function of time. An experiment to illustrate the effect of 'skin' formation. Measurements at $\omega = 10\ \text{rad s}^{-1}$, $\gamma = 10\%$.

Fig. 2, G' and G'' increase very rapidly from the start of the experiment when no attempt is made to reduce the 'skin' formation. The sudden depression of the values of the functions at about 700 s is thought probably to be due to the 'skin' bursting. The second set of experimental data shows that the solvent loss protocol is very effective in keeping G' and G'' constant for a period of time large enough to render all results obtained under this protocol accurate and reliable.

A dynamic strain sweep carried out at a frequency of $10\ \text{rad s}^{-1}$ is shown in Fig. 3(a). These data show that the oscillatory viscoelastic response is linear up to a strain of about 60%. The value of strain chosen for the linear viscoelastic frequency sweep was 10% and is shown in Fig. 3(b). It appears that the response of the concentrated cellulose acetate solution is similar to the classic behaviour of a thermoplastic melt with G'' dominating at low angular frequency and G' having a greater degree of importance at high frequencies. These oscillatory shear data points are used to determine the time constants (g_i, λ_i) by adopting a non-linear fitting procedure available in the Rheometrics software. The spectrum consists of 8 time constants and is represented in Fig. 3(c). Again this graph shows that the concentrated polymer solution has the characteristic feature of a molten polymer with the g_i decreasing monotonically over the time domain plotted. To check the consistency of this method the oscillatory moduli are regenerated from these coefficients and replotted as continuous lines in Fig. 3(c). A good fit to G'-G'' was obtained and the numerical values of the relaxation spectrum are listed in Table 1.

Step-strain data, shown in Fig. 3(d), show strain-softening at strains higher than 100%. It was also found that the stress relaxation curves obtained at various strains could be superimposed by a vertical shift after neglecting rise time errors. This is clear evidence that the material exhibits time-strain separability, i.e., the constitutive equation is factorable. With these step-strain measurements, the calculation of the damping function for the concentrated cellulose acetate solution was performed by utilising eq. (8). Linear regression was employed for the computation and for this polymer solution a k value of 0.33 fits the data best. The ratio of non-linear relaxation modulus to linear modulus at 20°C is given as a function of strain in Fig. 3(e). The error bars represent the standard deviation from the average value from the step strain data and the continuous curve shows the exponential fit with $k = 0.33$ according to eq. (8). It can be seen that the damping factor in general fits the data well. Typically, values of k of order 0.15 to 0.35 are found for some polyethylene melts [see, for example, Laun (1978). Booij and Palmen (1982) and Larson (1988)]. It is interesting to note that the damping factor for 25.5% cellulose acetate solution falls within this range.

Finally, the behaviour of the material under steady shear rate was predicted by the derived (g_i, λ_i) and k coefficients and compared with the experimental response as shown in Fig. 3(f). It is apparent from the measurements that the polymer solution is shear-thinning and there appears to be reasonably good agreement between the model and the experimental data. Experimental data is limited within the indicted range as the test material tends to move out of the plates of the RDSII Rheometer at high shear rates.

The results presented here show the model is capable of accurately characterising the essential elements of linear viscoelasticity and the non-linear steady shear response of the concentrated cellulose acetate solution. Furthermore, the rheological behaviour of the solution is observed to be similar to that of a polymer melt.

3. PROCESSING BEHAVIOUR USING THE MULTI-PASS RHEOMETER

Dynamic spectrometers such as the Rheometrics, Bohlin and Carrimed machines are very widely used to generate viscoelastic information from oscillatory data. The versatility of these rotational rheometers has often been extended to include the acquisition of non-linear steady shear measurements. Rotational rheometers, however, usually contain a free surface which may not be suitable for the measurements of sensitive fluids or solutions with volatile solvents. Alternatively, steady shear flow curves can be obtained from capillary rheometers, which have the advantage that the material under study is fully contained within the geometry. These capillary devices are, however, not usually capable of producing dynamic data.

Recently, a new Multi-Pass Rheometer II (MPRII) has been developed which is capable of obtaining both viscoelastic oscillatory and capillary data [see

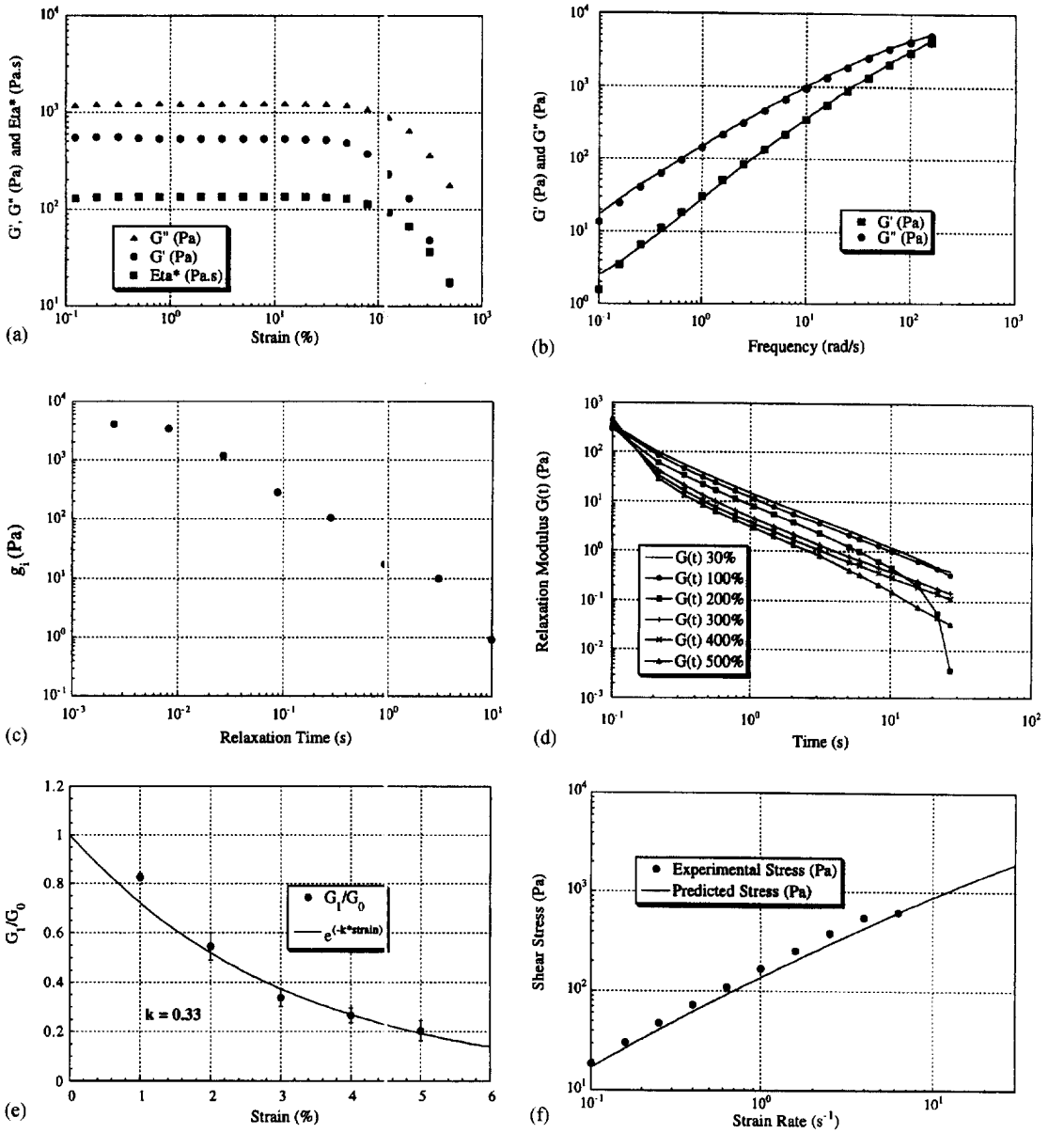

Fig. 3. Rheological characterisation of 25.5 wt% cellulose acetate–acetone solution at 20°C. (a) strain sweep, $\omega = 10$ rad s^{-1}, (▲) G'', (●) G', (■) η^*, (b) frequency sweep, $\gamma = 10\%$, (●) G'', (■) G', (– – – –) fit; (c) 'spectrum' of relaxation times; (d) step-strain data for strains of 30, 100, 200, 300, 400 and 500% from top to bottom, respectively, $k = 0.33$; (e) a plot to verify the Wagner's damping function, (●) ratio of average experimental non-linear relaxation modulus G_i to average experimental linear relaxation modulus G_0, (– – – –) fit; (f) steady shear measurements (●) and prediction with $k = 0.33$ (– – – –).

Mackley *et al.* (1995) and Mackley and Spitteler (1996)]. This apparatus is basically a capillary rheometer with two hydraulically driven pistons which force material through a detachable central test section as shown in Fig. 4. The piston movements are coupled and the fact that the multi-pass rheometer is an enclosed system also provides an attractive option for the rheological measurements of sensitive or volatile fluids and it is believed to offer an advantage over other machines in investigating the processing behaviour of rheologically difficult materials.

The multi-pass rheometer can be operated in two main modes:

(a) *Multi-pass steady mode*

When operating in a 'multi-pass steady' mode, fluid in the barrel is driven at a steady volumetric flowrate through the capillary section and the pressure difference across the capillary measured. This process can be repeated any number of times, hence 'multi-pass' rheometry. For a capillary of radius a and length L, for a fixed flow rate Q, the wall strain rate for a

Table 1. Constants (g_i, λ_i) of the relaxation spectrum and the damping coefficient k for a 25.5 wt% celllulose acetate–acetone solution at 20°C

Concentrated cellulose acetate–acetone
25.5 wt% Solution at 20°C
Damping factor, $k = 0.33$

g_i (Pa)	λ_i (s)
3997.2	0.002517
3416.2	0.0082083
1185.9	0.026825
280.77	0.087667
105.10	0.28650
17.580	0.93630
10.182	3.0599
0.91604	10.0

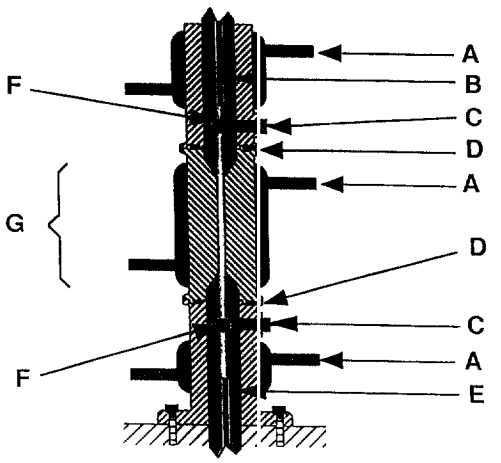

Fig. 4. A schematic diagram of Multi-Pass Rheometer. A. cooling/heating jackets, B. upper piston, C. pressure transducers, D. flanges incorporating O-rings, E. lower piston, F. thermocouples, G. capillary test section.

Newtonian fluid can be determined as follows:

$$-\dot{\gamma}_w = \frac{4Q}{\pi a^3}. \tag{10}$$

The wall shear stress τ_w is independent of the fluid's properties and can be related to the pressure difference over the capillary, providing entry effects are ignored, according to the following equation:

$$\tau_w = \frac{a\,\Delta P}{2L}. \tag{11}$$

The apparent viscosity of the fluid can then be evaluated yielding:

$$\eta = \frac{a^4 \Delta P}{8LR^2 v_p}. \tag{12}$$

where R is the radius of the piston and v_p the piston velocity. The pressure difference across the capillary is given by ΔP. Polymeric fluids are however usually non-Newtonian and therefore the Rabinowitsch–Mooney correction has to be made to evaluate the wall strain rate depending on the deviation of the Q–ΔP curve [see, for example, Rosen (1993)]:

$$-\dot{\gamma}_w = \frac{1}{\pi a^3}\left(3Q + \Delta P \frac{dQ}{d(\Delta P)}\right). \tag{13}$$

Therefore establishment of the Q–ΔP flow curve of the test material is essential as neglecting the Rabinowitsch–Mooney correction can sometimes lead to error. In addition, it may be necessary to consider entry and exits effects of the capillary although we have not considered this factor in this paper.

(b) *Oscillatory mode*

In this second mode of operation the pistons are again driven together with a sinusoidal velocity input. A phase angle δ, which is the phase angle difference between the applied sinusoidal strain and the resulting oscillatory stress (or the oscillating piston displacement and the differential pressure signal in this case), is calculated by a cross-correlation method. This method also generates the values of the applied and resulting amplitudes. By assuming that the piston position $x(t)$ takes the form $x_{max} \sin(\omega t + \varphi_x)$, where φ_x a phase angle due to the arbitrary point in time at which we start the data acquisition, the two following integrals can be evaluated [Mackley *et al.* (1995)]:

$$I_1 = \int_0^{2\pi} x(t) \sin \omega t \, d\omega t$$

and

$$I_2 = \int_0^{2\pi} x(t) \cos \omega t \, d\omega t. \tag{14}$$

Similarly, the following integrals can be determined for the differential pressure $P(t)$, where $P(t) = \Delta P_{max} \sin(\omega t + \varphi_p)$, with φ_p resulting from the phase angle δ and the arbitrary point in time in which we start acquiring the data:

$$I_3 = \int_0^{2\pi} P(t) \sin \omega t \, d\omega t$$

and

$$I_4 = \int_0^{2\pi} P(t) \cos \omega t \, d\omega t. \tag{15}$$

The phase angle δ is then given by

$$\delta = \varphi_x - \varphi_p = \arctan \frac{I_2}{I_1} - \arctan \frac{I_4}{I_3}. \tag{16}$$

The values of the amplitudes of displacement and differential pressure signals are:

$$x_{max} = \frac{1}{\pi}\sqrt{I_1^2 + I_2^2} \quad \text{and} \quad P_{max} = \frac{1}{\pi}\sqrt{I_3^2 + I_4^2}. \tag{17}$$

The storage and loss moduli can then be readily determined using the calculated parameters as follows:

$$G' = \frac{a^4 \Delta P_{max}}{8LR^2 x_{max}} \cos\delta \quad \text{and} \quad G'' = \frac{a^4 \Delta P_{max}}{8LR^2 x_{max}} \sin\delta. \tag{18}$$

where x_{max} is the centre to peak amplitude of the piston movement.

EXPERIMENTAL OBSERVATIONS USING THE MPRII

Experimental measurements on the multi-pass rheometer II (MPRII) were performed at 20°C in a capillary of length 40 mm and diameter 8 mm with the same solution of 25.5 wt% cellulose acetate. Dynisco pressure transducers of 35 bar were used for the data acquisition. An initial attempt to verify the self-consistency of the MPRII with the Rheometrics RDSII was achieved by performing dynamic oscillatory measurements and then comparing these results with those obtained from the RDSII.

Dynamic oscillatory data were obtained on the MPR by driving the pistons harmonically and measuring the resulting differential pressure signal. A graph of piston positions and differential pressure is shown in Fig. 5(a) where the frequency of the piston movement is 40 Hz corresponding to 250 rad s^{-1}. The continuous line shows the displacement of the top piston and the dotted line the measured differential pressure difference. It can be seen that the response to the harmonic deformation is also sinusoidal with a finite phase difference δ. The pressure signal is clear and reproducible rendering it easy to obtain both a peak pressure difference and phase angle. Having an enclosed structure, the MPR provides an effective way of eliminating the "skin" formation problem encountered with the measurements of cellulose–acetone system using the normal cone and plate rheometer. Figure 5(b) shows a time sweep for the material at a fixed frequency of 10 Hz. In this experiment, the fluid was driven sinusoidally with a maximum strain of 450% and the values of the dynamic moduli G' and

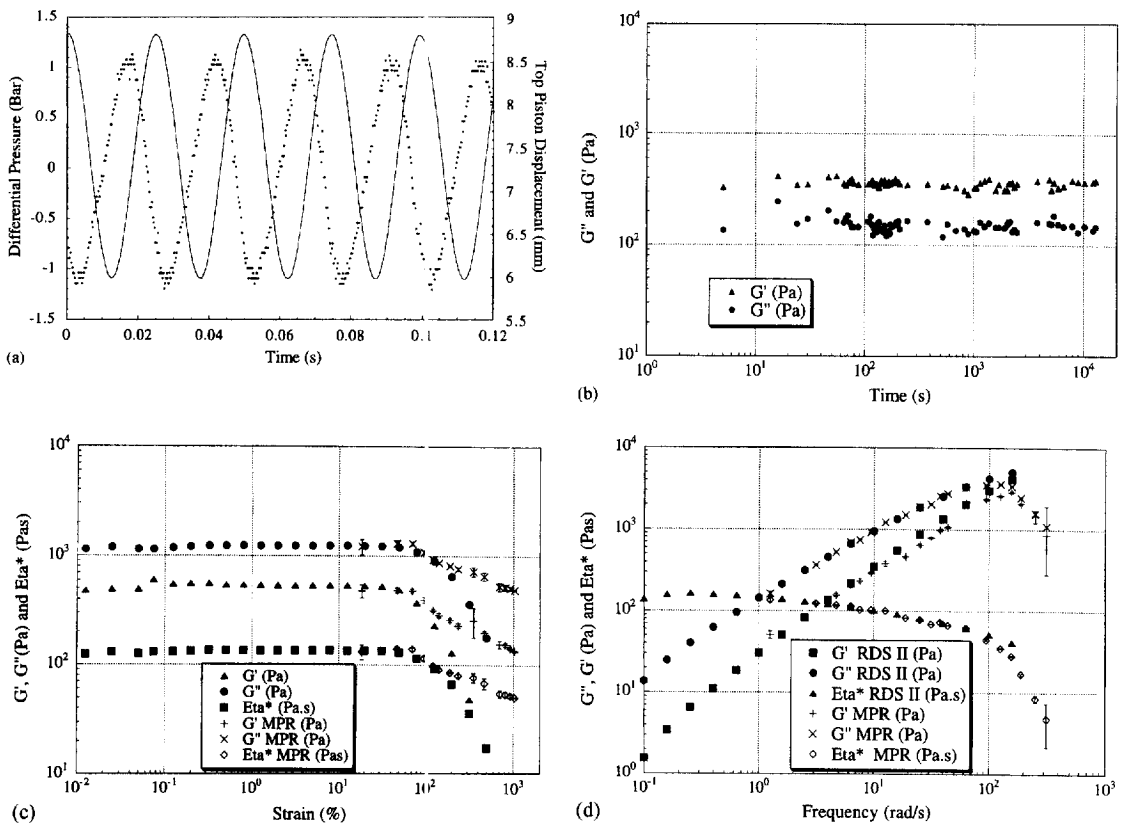

Fig. 5. MPRII oscillatory measurements on 25.5 wt% cellulose acetate-acetone solution at 20°C, length of capillary = 40 mm, diameter = 8mm, pressure transducer 35 bar, no prior pressuriation. (a) Differential pressure and top piston displacement as a function of time, the solid line corresponds to the piston position and the dotted line to the pressure difference. Centre to peak amplitude 1.4 mm, $\omega = 6.37$ rad s^{-1}. (b) Time sweep, maximum wall strain = 450%, $\omega = 10$ rad s^{-1}. (c) Strain sweep superposition, $\omega = 10$ rad s^{-1}, (▲) RDSII G', (●) RDSII G'', (■) RDSII η^*, (+) MPRII G', (×) MPRII G'', (○) MPR II η^*. (d) Frequency sweep superposition, $\gamma = 10\%$, (▲) RDSII G', (●) RDSII G'', (■) RDSII η^*, (+) MPRII G', (×) MPRII G'', (○) MPR II η^*.

G'' were followed with respect to time. A high amplitude and frequency were chosen to illustrate that the apparatus is still capable of generating reliable results even at such extreme conditions. The plot shows that the values of both the storage and the loss moduli are consistent for more than 10^4 seconds demonstrating the rheological stability of the fluid within the enclosed environment of the MPR.

A strain sweep was performed with a fixed frequency of 10 rad s^{-1} and the results were compared to the data from the RDSII as shown in Fig. 5(c). Because of the limits of pressure resolution at the low piston-amplitude end, data could only be acquired with piston amplitudes ranging from 0.1 to 0.45 mm. It can be seen that there is a very good correspondence between the RDSII data and the data obtained with the MPR except that the linear region seems to extend to slightly higher strains as measured with the MPR. Both systems indicate that the 25.5 wt% cellulose acetate solution has a linear region and the material starts to exhibit deviation from the linear viscoelastic response at a strain of about 60–70%. A frequency sweep in the 10% linear strain for the material on RDSII was shown in Fig. 3(b) earlier. We proceeded to produce these data with the multipass rheometer and a maximum linear strain of $\sim 45\%$ corresponding to a piston amplitude of 0.2 mm was chosen. Frequencies were selected between 0.15 and 55 Hz, corresponding to 1 and 350 rad/s. As presented in Fig. 5(d) there is good self-consistency between the two sets of data at frequencies below ~ 100 rad s^{-1}. At higher frequencies, the results from the RDSII and the MPR begin to diverge and this could be the result of a time resolution limitation at the high-frequency end as imposed by the pressure transducers.

From the results presented earlier, we are confident that there is reasonable consistency between the RDS II and the MPR and the latter is capable of producing reliable data. In addition to oscillatory measurements, it is possible to study the processing behaviour of the concentrated cellulose acetate solution by obtaining steady shear values by using the MPR. These results are shown in Fig. 6. When operating in the steady mode, the pistons are driven at a constant velocity to a specified amplitude. The pistons are then held for a chosen idle time and the motion then reversed. An example of steady shear measurements are shown in Fig. 6(a). The continuous line represents the displacement of the top piston. The piston velocity is chosen to be 40 mm s^{-1}, idle time 1.5 s, and the amplitude 10 mm. The dotted line shows the measured differential pressure data. It can be seen from the plot that there is a rapid pressure build up during the piston movement. Pressure relaxation starts to occur during the delay period upon the cessation of each piston movement. During the periods of rest, the differential pressure approaches zero. A high level of reproducibility for each pass is also indicated by the profiles shown in Fig. 6(a). The processing behaviour of 25.5 wt% concentrated cellulose acetate solution was studied by performing steady shear experiments on MPR with piston velocities ranging between 1 and 100 mm/s. Figure 6(b) shows the steady response of the material on MPR, where the Newtonian wall shear stress is plotted against shear rate. The steady shear measurements from the RDSII are shown on the same plot for comparison. The dotted line represents the flow curve predicted using spectrum of relaxation times and damping coefficient determined in earlier stages. It can be seen that a region of constant viscosity extends up to $\sim 2\,s^{-1}$, after which shear-thinning occurs. The results from the two different rheometers correspond well with each other and also with the predicted flow curve in the Newtonian plateau showing that the entry and exit effects of the MPR are insignificant. At shear rates above $100\,s^{-1}$, the results from MPR and the calculated values no longer compare. The viscosity as measured with the MPR decreases with increasing shear rate in a much smoother fashion, as compared to the RDSII, up to the maximum applied shear rate of $\sim 300\,s^{-1}$.

Rabinowitsch–Mooney corrected data are also incorporated in Fig. 6(b) as the polymer solution is non-Newtonian. The Q–ΔP relationship is obtained from the steady shear measurements on the MPR and the correction is performed on a spreadsheet according to eq. (13). In this case, the correction does not seem to modify the original results very much. In Fig. 6(b) we see that this correction is only significant at shear rates higher than $100\,s^{-1}$. In general, the correction leads to a better agreement between the MPR results and the prediction.

In Fig. 7 the steady shear apparent viscosity and the oscillatory complex viscosity from both the MPRII and the RDSII are plotted as a function of shear rate, and angular frequency, ω, respectively. It can be seen that the Cox–Merz rule as shown in eq. (7) appears to hold for this material on an empirical basis. These results give us further confidence in the reliability of both the steady shear and oscillatory data obtained on the equipment.

4. POLYFLOW MODELLING

The aim of our numerical simulation is to model the concentrated cellulose acetate solution flow within MPR using the experimental boundary conditions and compare the simulated results with the experimental observations, in order to check the applicability of the chosen constitutive equation and constitutive parameters. Moreover, we are aiming to show that the model is sufficient to describe the processing conditions as demonstrated by the multi-pass rheometer.

Numerical simulations were carried out using Polyflow software. Polyflow is a commercial finite element package which has been shown to be reliable for the modelling of steady polymer melt flow [see, e.g., DuPont and Crochet (1988), Van Gurp *et al.* (1993) and Feigel and Ottinger (1994)]. The principles of the finite element discretization concept, nevertheless, will

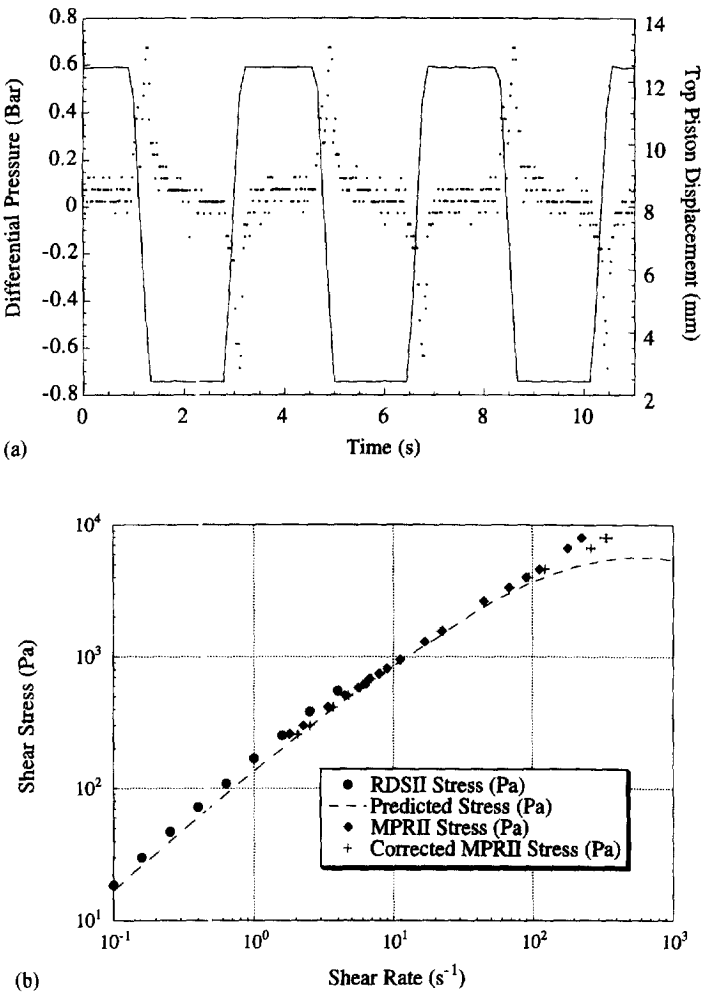

Fig. 6. MPRII steady experiments on 25.5 wt% cellulose acetate-acetone solution at 20°C, length of capillary = 40 mm, diameter = 8 mm, pressure transducer 35 bar, no prior pressurization. (a) Differential pressure and top piston displacement as a function of time, the solid line corresponds to the piston position and the dotted line to the resulting pressure difference, idle time = 1.5 s, piston velocity = 40 mm s^{-1}. (b) Steady shear measurement superposition, (□) MPR Wall shear stress vs Newtonian wall shear rate for piston velocity between 1 and 100 mm s^{-1}, (+) MPR data corrected with Rabinowitsch–Mooney correction, (◆) results as measured with the Rheometrics RDS-II rheometer, (- - - -) and the calculation of the flow curve using spectrum of relaxation times and damping coefficient.

not be discussed in this paper. The procedures for solving a general viscoelastic flow can be summarised as follows. Firstly, using a Polymesh program, a mesh in terms of the flow geometry is generated. Secondly, using the Polydata program, the mesh file is combined with the constitutive equation, material data and flow boundary conditions. This is then used as an input to run the Polyflow program. Finally, with a post-processing program, Polyplot, the results can be visualised.

The objective involves simulating the steady flow behaviour of the polymer solution in the MPR. All simulation results covered here are achieved with the simple shear experimental parameters for the 25.5 wt% cellulose acetate–acetone system as listed in Table 1. The finite mesh designed using Polymesh for the computation is shown in Fig. 8(a), and its geometry size is defined in Table 2 in comparison with the geometry size of the experimental capillary. The whole mesh is illustrated in the figure but in actual fact, only half of the geometry is needed for the simulation due to symmetry. The number of finite elements is also listed for the mesh.

An integral viscoelastic constitutive equation with the Wagner single parameter damping function as given in eq. (1) was selected for the computation. The flow boundary conditions we applied are as follows: A fully developed flow ($v_s = 0$, flow rate Q) as inflow, no slip ($v_s = 0$, $v_n = 0$) at the wall, a fully developed flow ($v_s = 0$, flow rate Q) as the outflow, and planar

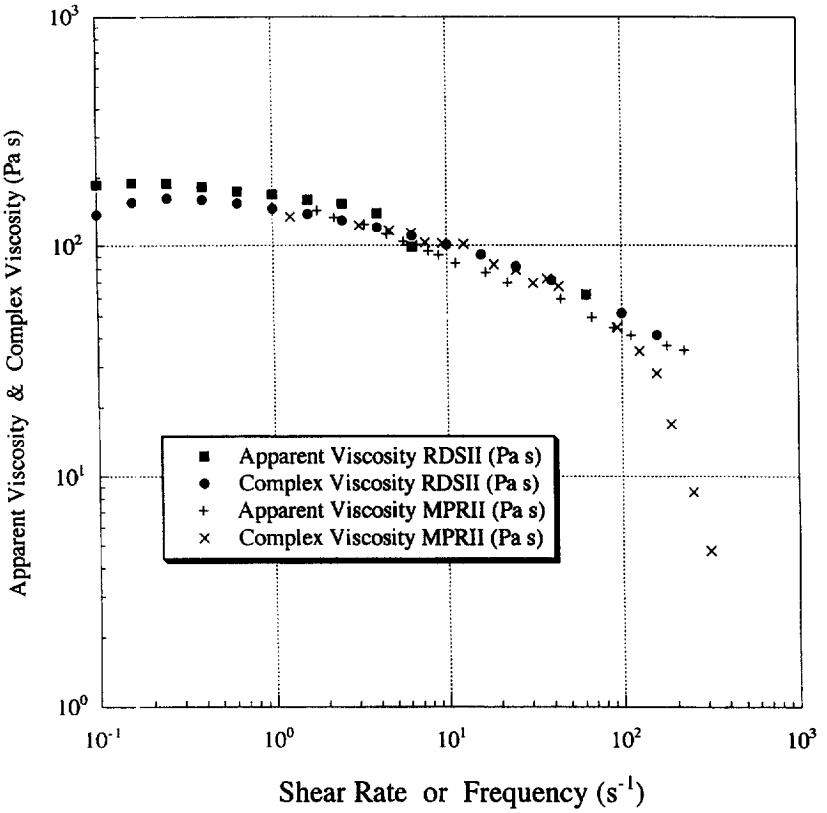

Fig. 7. Apparent viscosity η_{app} as a function of shear rate, (■) RDSII η_{app}, (+) MPRII η_{app}, and Complex viscosity η^* as a function of frequency, (●) RDSII η^*, (×) MPRII η^* at 20°C.

symmetry ($f_s = 0$, $v_n = 0$). Here, v is the velocity, f is the force, subscript s stands for tangential direction and subscript n stands for normal direction. Under experimental condition, the two servo-hydraulically driven pistons are synchronised to move together, pushing the test material across the capillary. The entry and exit lengths at both ends of the test section are therefore varying with time. This kind of flow boundary condition, however, is not an option in the Polydata program. The flow at either ends of the capillary was therefore assumed to be fully developed and the entry and exit lengths unchanging with time.

The finite element numerical technique used by Polyflow involves solving the field equations initially by first treating the polymer solution as a generalised Newtonian fluid. The viscosity was chosen to be 100 Pa s which is similar to the zero shear viscosity of the solution observed during steady shear experiments. The next step involves switching to the viscoelastic constitutive equation by the introduction of an evolutive parameter. At each stage of the evolution, a convergence criterion is applied, and using this method it is possible to obtain time-independent solutions of all the parameters and boundary conditions imposed. In our study, the flow rate Q was chosen as the evolutive parameter. The simulation began at an extremely low flow rate of 1×10^{-7} m^3 s^{-1} and that was increased progressively in 12 steps before the upper limit set at 1.1×10^{-5} m^3 s^{-1} was reached.

The Polyflow simulation results for $Q = 1 \times 10^{-7}$ m^3 s^{-1} are summarised in Figs 8(b)–(d). The streamline pattern, pressure contour and principal stress difference for the entire flow field can be viewed with the post-processing Polyplot program. From the streamline profile we deduced that the flow at both the entry and exit zones were quite smooth and there is no severe recirculation vortex. Figure 9 shows the pressure profiles plotted as a function of axial position starting form the upstream entry for the 12 different flow rates generated from the evolutive simulation. The pressure at the upstream entry position (= 0 m) is arbitrarily assigned as zero.

As seen from Fig. 9, the pressure begins to decay at the capillary entrance corresponding to position 0.01 m. The pressure continues to decrease linearly when it is flowing within the capillary and there is a small pressure decay at the exit. The overall pressure difference is also seen to increase with increasing flow-rate as expected. In Fig. 10, the numerically generated total pressure difference is compared with that obtained for different piston velocities and in general the agreement is found to be reasonable although the simulation over-predicts the pressure difference by

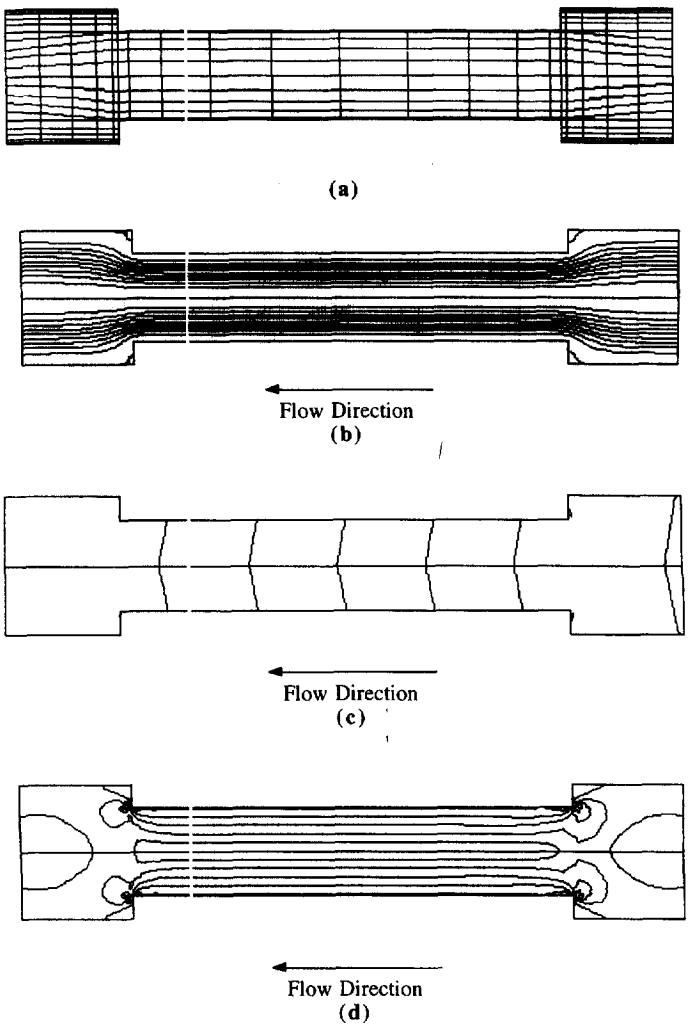

Fig. 8. Diagrams from Polyflow simulation. (a) View of the finite element mesh used in the computation, capillary length = 40 mm, capillary diamater = 8 mm, piston diameter = 12 mm. (b) The streamline diagram for $Q = 1 \times 10^{-7}\,m^3 s^{-1}$, flow from right to left. (c) The pressure contour for $Q = 1 \times 10^{-7}\,m^3 s^{-1}$, flow from right to left. (d) The principal stress difference profile from the simulation for $Q = 1 \times 10^{-7}\,m^3 s^{-1}$, flow from right to left. All rheological data g_i, λ_i and k taken from Figs 3(c) and 3(e).

Table 2. Experimental capillary geometry for the MPRII and 2D mesh size

	Mesh	Experimental
Length (mm)		
Entry length	10	> 10
Barrel length	40	40
Exit length	10	> 10
Radius of capillary	4	4
Radius barrel	6	6
Number of elements	150	—

a constant error of ~10% below $Q \sim 1 \times 10^{-5}\,m^3 s^{-1}$. This error could be caused by the disparity between the experimental and simulation flow boundary conditions.

5. DISCUSSION AND CONCLUSION

This paper has shown that the rheological behaviour of a concentrated cellulose acetate solution with a weight solid fraction of about 25% can be predicted successfully by a model originally developed by Wagner (1976) for polyethylene melts. We have observed that the polymer solution behaves similarly to a melt in more than one way. Firstly, the g_i coefficients of its relaxation modes decrease montonically over the time domain plotted which is a characteristic feature of a molten polymer. Secondly, the value of the damping factor k is typical for that of some polyethylene melts. Both these factors suggest that the cellulose acetate polymer chains adopt an entangled random configuration in a similar way to say, polyethylene or polystyrene chains.

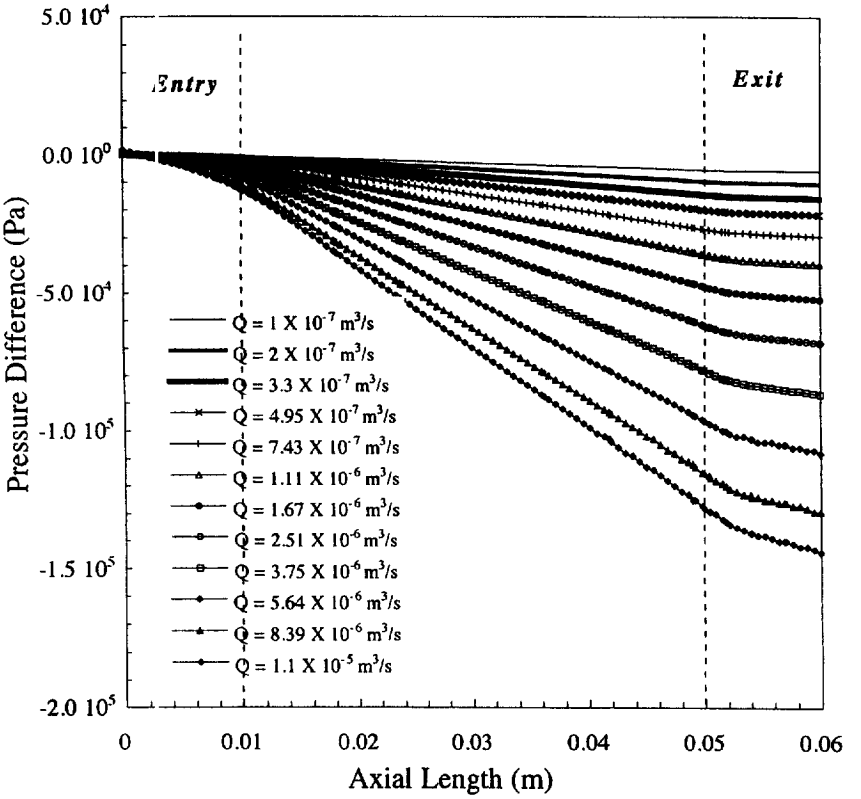

Fig. 9. Polyflow simulation on MPRII results, a graph of centreline pressure difference as a function of the axial length across the capillary, for 12 different flow-rates, capillary length = 40 mm, capillary diameter = 8 mm, piston diameter = 12 mm.

A protocol which involves silicon oil coating and acetone saturation has been developed for the rheological measurements of the volatile cellulose acetate solution, using a conventional Rheometrics Dynamics Spectrometer RDSII to reduce the rate of 'skin' formation. The newly developed Multi-Pass Rheometer (MPR) is however an enclosed system and is therefore free from these solvent evaporation difficulties. The rheological measurements reported in this paper using the MPR have shown that the machine is both reliable and gives good self-consistency with the simple shear RDSII data.

Processing measurements have been carried out using the MPR which we have then modelled using a Polyflow simulation. The discrete relaxation spectrum data with eight time constants and the damping coefficient from simple shear flow have been used as input information for the simulation to generate a pressure/flowrate prediction and there is good agreement between the experimental data and simulated results. The Rabinowitsch–Mooney correction has been performed on the MPRII steady shear measurements, however, it was shown to be significant only at higher shear rates. From the results, we are confident that Polyflow simulations are accurate and could be extended with benefit to more complex engineering situations and used in a design role for optimisation of processing.

The viability of the multi-pass rheometer has been demonstrated in this paper and the cellulose acetate solution has acted as a very useful model system. We believe that multi-pass rheometry is capable of carrying out a broad set of rheological measurements under controlled conditions. The technique is potentially very flexible as a wide range of insert test sections can be used. The device could in the future be extended to more complex systems, different temperatures and other flow geometries. The independent control of mean pressure is another useful feature of the MPR although it has not been specifically exploited in this paper.

Rather surprisingly, we have found that the rheology of the cellulose acetate solutions whilst under test and operated in the enclosed environment of the MPR, was both stable in terms of time and process history. In the future it would be of interest to explore less stable systems where either time and/or process history would affect the measured rheology.

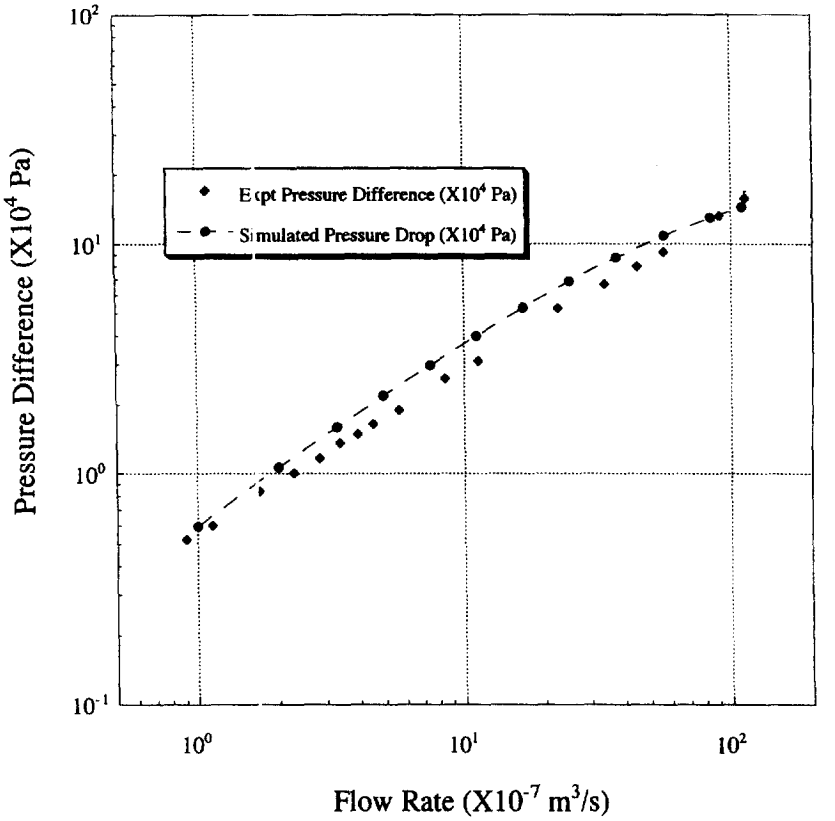

Fig. 10. A comparison between the Polyflow simulated results against the MPRII experimental data for steady shear flow at 20°C, centreline pressure difference as a function of flow rate across the capillary, capillary length = 40 mm, capillary diameter = 8 mm, piston diameter = 12 mm, (◆) MPRII ΔP, (– –●– –) simulated ΔP.

Acknowledgements

We wish to thank Courtaulds PLC for financial support and we are particularly grateful to Tom Dovey, Anthony Higgins, Brian McGarey and John Newbury for useful background discussions on cellulose acetate systems. WKW also wishes to thank the Cambridge Commonwealth Trust and Trinity College for additional financial support.

NOTATION

a	radius of capillary, mm
f	force, N
g	relaxation strength, Pa
G	relaxation modulus, Pa
G'	storage modulus, Pa
G''	loss modulus, Pa
k	damping coefficient
L	length, m
ΔP	pressure difference, Pa
Q	flow rate, $m^3 s^{-1}$
R	radius of piston, mm
t	time, s
v	velocity, mm s^{-1}
x	piston position, mm

Greek letters

γ	shear strain
$\dot{\gamma}$	shear rate, s^{-1}
δ	phase angle
η	viscosity, Pa s^{-1}
η^*	complex viscosity, Pa s
λ	relaxation time, s
τ	shear stress, Pa
φ	phase angle between piston position and pressure difference
ω	frequency, rad s^{-1}

REFERENCES

Aldhouse, S. T. E., Mackley, M. R. and Moore, I. P. T. (1986) Experimental and linear viscoelastic stress distribution measurements of high density polyethylene flowing into and within a die. *J. non-Newt. Fluid Mech.* **21**, 359–376.

Baumgaertel, M. and Winter, H. H. (1992) Interaction between continuous and discrete relaxation time spectra. *J. non-Newt. Fluid Mech.* **44**, 15–36.

Booij, H. C. and Palmen, J. H. M. (1982) Some aspects of linear and non-linear viscoelastic behaviour of polymer melts in shear. *Rheol. Acta* **21**, 376–387.

Cox, W. P. and Merz, E. H. (1958) Correlation of dynamic and steady viscosity. *J. Polym. Sci.* **28**, 612.

DuPont, S. and Crochet, M. J. (1988) The vortex growth of a K-BKZ fluid in an abrupt contraction. *J. non-Newt. Fluid Mech.* **29**, 81–91.

Feigl, K. and Ottinger, H. C. (1994) The flow of a LDPE melt through an axisymmetric contraction:

A numerical study and comparison to experimental results. *J. Rheol.* **38**, 847–874.

Ferry, J. D. (1980) *Viscoelastic Properties of Polymers, 3rd ed.* Wiley, New York.

Griswold, P. D. and Cuculo, J. A. (1974) An experimental study of the relationship between rheological properties and spinnability in the dry spinning of cellulose acetate-acetone solutions. *J. Appl. Polym. Sci.* **18**, 2887–2902.

Johnston, H. K. and Sourirajan, S. (1973) Viscosity-temperature relationships for cellulose acetate-acetone solutions. *J. Appl. Polym. Sci.* **17**, 3717–3726.

Larson, R. G. (1988) *Constitutive Equations for Polymer Melts and Solutions.* Butterworths, Boston.

Laun, H. M. (1978) Description of the non-linear shear behaviour of a low density polyethylene melt by means of an experimentally determined strain dependent memory function. *Rheol. Acta* **17**, 1–15.

Mackley, M. R., Marshall, R T. M. and Smeulders, J. B. A. F. (1995) The multi-pass rheometer. *J. Rheol.* **39**(6), 1293–1309.

Mackley, M. R., Marshall, R. T. M., Smeulders, J. B. A. F. and Zhao, F. D. (1994) The rheological characterization of polymeric and colloidal fluids. *Chem. Engng Sci.* **49**, 2551–2565.

Mackley, M. R. and Spitteler, P. H. J. (1996) Experimental observations on the pressure-dependent polymer melt rheology of linear low density polyethylene, using a multi-pass rheometer. *Rheol. Acta* **35**, 202–209.

Moore, W. R. and Brown, A. M. (1959) Viscosity-temperature relationships for dilute solutions of cellulose derivatives: I. Temperature dependence of solution viscosities of ethyl cellulose. *J. Colloid Sci.* **14**, 1–12.

Moore, W. R. and Brown, A. M. (1959) Viscosity-temperature relationships for dilute solutions of cellulose derivatives: II. Intrinsic viscosities of ethyl cellulose. *J. Colloid Sci.* **14**, 343–353.

Papanastasiou, A. C., Scriven, L. E. and Macosko, C. W. (1983) An integral constitutive equation for mixed flows: Viscoelastic Characterization. *J. Rheol.* **27**(4), 387–410.

Rosen, S. L. (1993) *Fundamental Principles of Polymeric Materials, 2nd ed.* Wiley-Interscience, New York.

Soskey, P. R. and Winter, H. H. (1984) Large step shear strain experiments with parallel-disk rotational rheometers. *J. Rheol.* **28**(5), 625–645.

Van Gurp, M., Breukink, C. J., Sniekers, R. J. W. M. and Tas, P. P. (1993) Rheological characterization of low density polyethylene in planar extension using rheo-optics. *SPIE, Laser Anemometry Adv. Appl.* **2052**, 297–304.

Wang, C. S. and Fried, J. R. (1992) Viscoelastic properties of concentrated cellulose acetate solutions. *J. Rheol.* **36**(5), 929–944.

Wagner, M. H. (1976) Analysis of time-dependent non-linear stress-growth data for shear and elongational flow of a low-density branched polyethylene melt. *Rheol. Acta* **15**, 136–142.

Wagner, M. H. (1979) Zur Netwerktheorie von polymer-schmelzen. *Rheol. Acta* **18**, 33–50.